

Published in final edited form as:

Contrast Media Mol Imaging. 2012 ; 7(4): 363–372. doi:10.1002/cmimi.494.

Assessment and comparison of magnetic nanoparticles as MRI contrast agents in a rodent model of human hepatocellular carcinoma

Lihong Bu, MD, PhD^{1,2,3}, Jin Xie, PhD², Kai Chen, PhD³, Jing Huang, PhD³, Zoraida P. Aguilar, PhD⁴, Andrew Wang, PhD⁴, Kin Wai Sun, PhD⁵, Mei-Sze Chua, PhD⁵, Samuel So, MD, PhD⁵, Zhen Cheng, PhD², Henry S. Eden, MD, PhD², Baozhong Shen, MD, PhD¹, and Xiaoyuan Chen, PhD²

¹Department of Radiology, the Fourth Hospital of Harbin Medical University, Heilongjiang, China

²Laboratory of Molecular Imaging and Nanomedicine (LOMIN), National Institute of Biomedical Imaging and Bioengineering (NIBIB), National Institutes of Health (NIH), Bethesda, MD, USA

³Molecular Imaging Program at Stanford (MIPS), Department of Radiology, Stanford University School of Medicine, Stanford, CA, USA

⁴Ocean NanoTech, LLC, Springdale, AR, USA

⁵Asian Liver Center, Department of Surgery, Stanford University School of Medicine, Stanford, CA, USA

Abstract

PURPOSE—The purpose of this study was to synthesize, characterize and tailor the surface properties of magnetic nanoparticles with biocompatible copolymer coatings and to evaluate the efficiency of the resulting nanoconjugates as magnetic resonance imaging (MRI) contrast agents for liver imaging.

METHODS—Magnetic nanoparticles with core diameters of 10 and 30 nm were synthesized by pyrolysis and were subsequently coated with a copolymer containing either carboxyl (SHP) or methoxy groups (SMG) as termini. All four formulas, and ferumoxides (Feridex I.V.®), were individually injected intravenously into separate, normal Balb/C mice (at 2.5, 1.0, and 0.56 mg Fe/kg), and the animals underwent T₂-weighted MRI at multiple time points post injection (p.i.) to evaluate the hepatic uptake and clearance. Furthermore, we compared the abilities of the new formulas and Feridex to detect tumors in an orthotropic Huh7 tumor model.

RESULTS—TEM revealed a narrow size distribution of both the 10 nm and 30 nm nanoparticles, in contrast to a wide size distribution of Feridex. MTT, apoptosis and Cyclin/DNA flow cytometry assays showed that the polymer coated nanoparticles had no adverse effect on cell growth. Among all the tested formulas, including Feridex, SHP-30 showed the highest macrophage uptake at the *in vitro* level. *In vivo* MRI studies on normal mice confirmed the superiority of SHP-30 in inducing hypointensities in the liver tissue, especially at clinical dose (0.56 mg Fe/kg) and 3T field. SHP-30 showed better contrast-to-noise ratio (CNR) than Feridex on the orthotropic Huh7 tumor model.

CONCLUSION—SHP-30 was found to be an efficient contrast agent for liver MR imaging. The success of this study suggests that by improving the synthetic approach and by tuning the surface properties of IONPs, one can arrive at better formulas than Feridex for clinical practice.

Keywords

Iron oxide nanoparticle (IONP); hepatocarcinoma (HCC); magnetic resonance imaging (MRI); liver contrast agent

INTRODUCTION

Superparamagnetic iron oxide nanoparticles (IONPs) have long been used as magnetic resonance (MR) contrast agents (1). They were widely investigated for liver imaging due to their greater uptake by Kupffer cells than by other cell types (2–3). Such a passive targeting feature, i.e. the overwhelming uptake of IONPs by the immune system, has also been extended to image other organ types, such as spleen, bone marrow and lymph nodes. During the past decade, there have also been efforts to link IONPs with vector ligands, such as antibodies, peptides and aptamers, to confer the targeting specificity of the nanoconjugates (4–7). Furthermore, IONPs have been increasingly investigated as promising biomaterials for targeted drug delivery, cell separation, induction of hyperthermia, cellular magnetic labeling and for magnetic sensor applications (1,8–11).

The IONP formulas currently used in the clinic are almost exclusively made by co-precipitation, a protocol established over two decades ago. The synthesis is efficient and of high throughput; the drawback of the method, however, is that it is suboptimal in controlling the qualities of the final products, including their average size, size distribution and crystallinity, as manifested by their relatively low T_2 contrast capability and inability to be injected intravenously. Since the bolus injection of Feridex is not recommended because of possible side effects which may be related to their large hydrodynamic size and wide size distribution, dynamic contrast-enhanced imaging has not been possible so far. Recent discontinuation of Feridex further underscores the urgency of developing IONPs with higher magnetization, better water solubility and superior biocompatibility (12–13).

We herein report one of our efforts along this line. Instead of using the traditional co-precipitation method, we adopted a pyrolysis recipe to synthesize IONPs. We and others have demonstrated that IONPs produced by such a method possess better crystallinity and are therefore superior to those made from co-precipitation in shortening spin-spin relaxation time (11). Besides, compared with the traditional co-precipitation methods, the pyrolysis method provides better control over particle size (1,14–16). In the current study, we prepared IONPs with core sizes of 10 and 30 nm by following a previously reported protocol (17). We then imparted a biocompatible tri-block copolymer (18) onto the as-synthesized IONPs to confer water solubility to the IONPs. To investigate the impact of PEGylation, we coupled NH_2 -PEG2000-OMe to the carboxyl groups of the polymer on the IONP surface. Four types of IONPs were thus produced: (1) 10 nm core with carboxylate groups on the surface (SHP-10); (2) 10 nm core with methoxy PEG groups on the surface (SMG-10); (3) 30 nm core with carboxylate groups on the surface (SHP-30); and (4) 30 nm core with methoxy PEG on the surface (SMG-30). We then compared these four formulas with Feridex *in vitro* to assess their uptake by macrophages and *in vivo* to evaluate their abilities and sensitivities as liver contrast agents.

MATERIALS AND METHODS

Synthesis, surface modification and characterizations of IONPs

All chemicals were purchased from Aldrich. IONPs with uniform size distribution were prepared as reported and suspended in hexane or chloroform (17). The hydrophobic nanoparticles were rendered water soluble by a polymer coating method developed by Duan

et al. (18). SMG was synthesized via 1-ethyl-3-(3-dimethylaminopropyl)carbodiimide hydrochloride (EDC) coupling using NH₂-PEG2000-OMe. The morphology of the IONPs was examined by TEM (CM 20 microscope, Philips). The hydrodynamic sizes as well as the zeta potentials of the IONPs were examined on a DynaPro molecular sizing instrument (Wyatt Technology Corp.) at 25 °C.

Cellular Uptake Assay

The cellular uptake studies were performed on RAW 264.7 cells (mouse macrophage cell line) and Huh7 cells (human hepatocellular carcinoma cell line). Both cell lines were obtained from the American Type Culture Collection (ATCC). For cell culture, 0.5×10^6 cells were initially seeded in 6 well plates and were cultured in folate-free RPMI-1640 medium containing 10% FBS and 1% penicillin/streptomycin for 24 h. The growth medium was then aspirated and the cells were washed twice with PBS. For cell uptake studies, each of the five formulas (SHP-10, SHP-30, SMG-10, SMG-30 and Feridex) was added, in folate-free RPMI, to the 6-well plates. The final Fe concentration was 0.01 mg Fe/ml, and the incubation proceeded for 4, 8 and 24 h. At the end of the incubation, the medium was aspirated and the cells were washed three times with PBS. The cells were then detached and counted. The Fe uptake was quantified by inductively coupled plasma-atomic emission spectrometry (ICP-AES). The ICP samples were prepared by subjecting a known number of cells to nitric acid with heat (100 °C) for 2 h. The resulting solution was then diluted to a volume of 6 ml for analysis. The tests were performed in triplicate.

Cytotoxicity

The cytotoxicity study was performed with RAW 264.7 cells using a 3-(4,5-dimethylthiazol-2-yl)-2,5-diphenyl tetrazolium bromide (MTT) assay (Roche Molecular Biochemicals, Indianapolis, Indiana). In brief, RAW 264.7 cells were seeded at a concentration of 4×10^3 cells/well to 96 well plates and were allowed to attach overnight. The next day, each of the five formulas was added at a pre-determined Fe concentration (from 0.08 to 50 µg Fe/ml), and the cells were incubated for 24 h. After incubation, the cells were washed three times with PBS, and MTT was added at a final concentration of 0.5 mg/ml. The cells were incubated for 1 h at 37 °C with 5% CO₂. Subsequently, the medium was aspirated, and 200 µl DMSO was added to each well. The absorbance at 570 nm was measured 1 h later.

The effect of IONPs on cell cycle distribution was determined by FCM after staining the cells with PI. Briefly, 5×10^5 cells were seeded in 25 cm² culture flasks and allowed to attach for 6 h incubation and FBS free medium replacement for overnight. The medium was replaced with fresh complete medium containing each of the three formulas (Feridex, SHP-30 and SMG-30) with pre-determined Fe concentration (from 0.08 to 50 µg Fe/ml). PBS was added as blank control. After incubation for 24 h at 37 °C, floating and adherent cells were collected, washed with ice-cold PBS, and fixed with 70% ethanol for at least 12 h at 4 °C. The cells were then treated with 50 µg/ml PI at a density of 1×10^6 cells/ml for 30 min, and the stained cells were analyzed using a BD FACSCalibur flow cytometer. Data acquisition (10,000 events for each sample) was performed using Cell Quest software (Becton Dickinson, USA).

The apoptotic rate was measured by flow cytometry according to the instructions provided by the annexin V-FITC kit. In brief, after incubation with IONPs at a pre-determined Fe concentration (from 0.08 to 50 µg Fe/ml), cells were harvested after digestion with 0.25% trypsin, washed three times with ice-cold PBS containing calcium, and resuspended in 500 µl binding buffer at a concentration of 1×10^6 cells/ml, in which 500 µl of cell suspension was added in a 5 ml flow cytometry tube. Annexin V-FITC (50 µg/ml, 5 µl) and PI (50 µg/

ml, 5 μ l) were added and incubated for 30 min at room temperature in the dark. PBS was considered as blank control. Quantitative analysis of apoptotic level was performed using a FCM. The apoptotic percentage of 10,000 cells was determined.

Study Using a Phantom

A study using a phantom was performed to assess the efficacy of the probes as T_2 -weighted MRI contrast agents. All the five formulas with various iron concentrations (15, 7.5, 3.75, 1.875, 0.938, 0.469 and 0.234 μ g/ml) were suspended in 1% agarose gel in 300 μ l PCR tubes. The tubes were embedded in a home-made tank, which was designed to fit the MRI coil that was filled with 1% agarose gel. The tank, along with the PCR tubes, was inserted into the MRI coil with the long axis of the vials parallel to the static magnetic field, and a transverse tomographic plane orientation was used. T_2 -weighted MRI images were acquired on a GE 7.0 T small animal MRI system with multi echo turbo spin echo (TSE) sequence and the following parameters: TR = 3000 ms; TE = 20, 40, 60, 80, 100, and 120 ms; flip angle = 30°; FOV = 6 \times 6, 256 \times 256 matrix; slice thickness = 1 mm; and NEX = 1. A first-order shim process was applied, and the phantoms were imaged at room temperature. To determine whether the relaxivity of the IONPs vary with field strength, phantom studies were repeated on a GE 3.0 T clinical MRI system with a dedicated small animal coil (Chenguang Med Tech, Shanghai, China) with identical MR pulse parameters as the 7.0 T small animal MRI system.

Animal model preparation

Normal Balb/c mice (6–7 weeks old, Harlan) with a body weight of 20.7 ± 1.8 g, were used in the investigation (3 animals for each contrast agent, dose and magnetic field strength). Athymic nude mice were used to establish the orthotropic hepatocellular carcinoma model. All animal studies were conducted in accordance with the principles and procedures outlined in the Stanford University Institutional Animal Care and Use Committee (IACUC).

The Huh7 cells were transfected with firefly luciferase reporter gene. The tumors were established by subcutaneous injection of 5×10^6 cells in 100 μ l PBS into the front flank of each mouse. When the tumor volume reached 700–800 mm³ (1–2 wk after inoculation), the tumor was carefully excised and cut into small tissue fragments of 1 mm³ devoid of necrotic tissue. The orthotropic hepatocellular carcinoma model was generated by transplanting a tumor tissue fragment into the left lobe of each mouse's liver by surgery. Mice were anesthetized with isoflurane (IsoFlo; Abbott Laboratories) inhalation and were put in a supine position. The abdomen was sterilized with iodine and alcohol swabs. A left subcostal incision was made to expose the left lobe of the liver. A small cut on the Glisson's capsule of the left lobe was then performed. One piece of the above tumor tissue fragment was inserted into the incision on the liver of each mouse. The fragment was then sutured in place using a 6-0 silk. The abdomen was closed with a 5-0 silk suture. The tumor growth was monitored by bioluminescence (BLI) imaging on a Xenogen IVIS device (Caliper Lifesciences). At about 15 min prior to imaging, animals were injected i.p. with D-luciferin at a dose of 150 mg/kg in Dulbecco PBS (DPBS) with 0.5% BSA. The mice underwent MR imaging 1–2 wks after implantation.

In vivo MRI and data analysis

For imaging of normal mice, the mice were first anesthetized with 1–2% isoflurane in 1:2 O₂:N₂. Subsequently, each of our four formulas and Feridex was injected into separate Balb/C mice through the tail vein at a dose of 2.5, 1, or 0.56 mg Fe/kg. T_2 -weighted fast spin-echo imaging was performed at multiple time points post-injection (p.i.), namely at 10 min, 1 h, 24 h, 72 h, 1 wk and 2 wks, with the following parameters: for 7.0 T small animal MRI, TE = 40 ms, TR = 3000 ms, thickness = 1 mm, FOV = 6 \times 6, NEX = 1.0, echo = 1/1; for 3.0

T clinical MRI, TE = 40 ms, TR = 4000 ms, thickness = 1 mm, FOV = 6 × 6, NEX = 3.0, echo = 1/1. For the imaging of the orthotropic Huh7 tumor model, all of the particles were administered at a dose of 2.5 mg Fe/kg. T₂-weighted fast spin-echo images were acquired by the 7.0 T MR system pre- and 10 min and 1 h post-injection using the same parameters described above.

From each data set, one slice that showed the liver tumor and a larger portion of normal liver tissue without partial volume effects was selected to determine the signal intensity of liver (SI_{liver}), tumor (SI_{tumor}), and noise (SI_{noise}) by standard region-of-interest (ROI) measurements. The size of the ROI for liver and tumor was 49.7 ± 11.2 pixels and that for the noise was about 100 pixels. The measurements were performed by two experienced investigators in consensus with regard to the location and size of the region of interest. For the measurements of SI_{liver}, larger blood vessels were avoided. Moreover, larger necrotic areas were likewise excluded from the SI_{tumor} region of interest on T₂-weighted fast spin-echo images. SI_{noise} was determined anterior to the mice in the frequency-encoding direction to exclude motion artifacts induced by respiration or vessel pulsation. SI_{noise} in the phase-encoding direction was not included in the analysis since the aim of our study was to evaluate the signal intensity changes induced by the various contrast media, rather than to compare pulse sequences. The measured signal intensity values were used to calculate signal-to-noise ratio (SNR) for the liver as $SNR_{liver} = SI_{liver}/SI_{noise}$ and for the tumor as $SNR_{tumor} = SI_{tumor}/SI_{noise}$ for each animal and time point. The contrast between liver and tumor was determined by calculating the contrast-to-noise ratio (CNR) as $CNR = (SI_{liver} - SI_{tumor})/SI_{noise}$.

Statistical Analysis

All tests of significance were two sided, and differences were considered statistically significant when $P < 0.05$. Graph-Pad Prism software was used for all analyses. For comparison of SNR and CNR values of the contrast media, a two-factorial nonparametric analysis of variance was performed for the different image acquisition time points and contrast medium groups to take into account the correlated nature of the repeated measurements. For comparison of SNR and CNR values of the contrast media, a paired t-test was used.

RESULTS

Preparation and characterizations of water soluble IONPs

The IONPs were prepared by following a reported protocol (17). The exact reaction conditions to obtain nanoparticles were as the following: for 10 nm IO, 0.18 mole of iron oxide powder was added to the mixture of 0.72 mole of oleic acid and 300 g octadecene in 3 l three-necked flask under N₂. The solution was heated to above 300 °C for 30 min to obtain 10 nm IO nanoparticles; for 30 nm IO, 0.18 mole iron oxide powder was added to mixture of 1.44 mole oleic acid and 300 g octadecene in 3 l three-necked flask under N₂, the solution was heated to above 300 °C for 2 h to obtain 30 nm IO nanoparticles. The core size of IONPs was determined by TEM analysis. As displayed in Fig. 1, both types of IONPs demonstrated a very narrow size distribution.

Such as-synthesized IONPs were coated with a thick layer of hydrocarbon chain and were not water soluble. A copolymer of poly(maleic acid) and octadecene (PMO) (18), was coated onto the IONP surface via hydrophobic interactions with the surfactant. This copolymer has multiple carboxylate groups on its surface, which helps to suspend the IONPs (SHP-10 and SHP-30) in aqueous solution and allows them to be further coupled with other biomolecules by forming an amide bond. In the current study, we introduced NH₂-

PEG2000-OMe onto both SHP-10 and SHP-30 to produce SMG-10 and SMG-30. Such a conjugation led to a significant drop of zeta potential (Table 1). Meanwhile, DLS results showed that the hydrodynamic sizes were increased from 23.1 nm (for SHP-10) to 25.0 nm (for SMG-10), and from 49.1 nm (for SHP-30) to 63.8 nm (for SMG-30) (Fig. 1c,d). Note that the average hydrodynamic sizes of all 4 formulas were considerably smaller than Feridex. To check the stability of the nanoparticles, we placed all 4 new particle formulas, as well as Feridex, in a tightly sealed container for 1 year at 4 °C and no precipitation was found in any of these formula.

Cellular uptake and cytotoxicity assays

As shown in Figure 2, all the nanoparticle formulas, including Feridex, showed greater uptake by RAW 267.3 than by Huh7 cells. Although all the formulas showed a comparable uptake by Huh7 cells, we observed a big difference in terms of macrophage uptake. Specifically, while both SHP-10 and SHP-30 showed higher uptake than Feridex, SMG-10 and SMG-30 showed less uptake than Feridex at all the time points examined. After 24 h incubation, the uptake of nanoparticles was found to be 7.34 ± 0.09 pg Fe/cell for SHP-10, 11.78 ± 0.26 pg Fe/cell for SHP-30, 6.53 ± 0.34 pg Fe/cell for Feridex, 4.66 ± 0.26 pg Fe/cell for SMG-10, and 5.40 ± 0.07 for SMG-30. These results demonstrate that both surface charge and nanoparticle size play important roles in determining the cellular uptake rate. The negatively charged SHP-10 and SHP-30 have greater uptake by macrophages than the neutral SMG-10 and SMG-30. Meanwhile, the larger particles appear to have more macrophage uptake than smaller particles with the same surface coating. In order to determine whether the addition of IONPs induced cell apoptosis, flow cytometry was conducted in both IONP and PBS treated RAW 264.7 cells. The cell apoptosis rates were shown in Figure 2c. No statistical difference between the PBS control and IONP treated cells, indicating that IONPs don't result in cell apoptosis. We designed experiments to determine whether IONPs suppress RAW 264.7 cells proliferation. As can be seen in Fig. 2d, a 24 h incubation on RAW 264.7 cells with increasing doses of IONPs, flow cytometry assay showed no statistical difference in the proportion of G2/M phase between the PBS group and each group after the treating with different amount of IONPs, which proved that IONPs have no influence on RAW 264.7 cell proliferation. Notably, at the studied concentrations, there was no apparent effect on cell growth for any of the nanoparticles tested (Fig. 2e).

Phantom study

All four formulas (SHP-10, SHP-30, SMG-10, and SMG-30), as well as Feridex, showed concentration dependent hypointensities in T_2 -weighted maps as measured by the 7.0 T small animal MRI system. The r_2 values derived from $1/T_2$ vs. [Fe] curves were 201.5 ± 7.1 $\text{mM}^{-1}\text{s}^{-1}$ for SMG-10, 214.12 ± 4.0 $\text{mM}^{-1}\text{s}^{-1}$ for SMG-30, 212.67 ± 5.8 $\text{mM}^{-1}\text{s}^{-1}$ for SHP-10, 230.3 ± 1.5 $\text{mM}^{-1}\text{s}^{-1}$ for SHP-30 $\text{mM}^{-1}\text{s}^{-1}$ and 152.2 ± 2.5 $\text{mM}^{-1}\text{s}^{-1}$ for Feridex (Fig. 3). All four formulas had clearly better T_2 contrast than Feridex (Table 2, $P < 0.05$). Among the four formulas, larger core size particles appeared to have higher r_2 values than the smaller ones. A slight decrease of r_2 value was observed when the SHP particles were converted to PEGylated SMG particles. This is likely attributable to the increased size caused by PEGylation and, consequently, increased exclusion radius of protons from the magnetic field (19). The same phantom study was repeated at 3.0 T clinical MRI system with r_2 values of 211.2 ± 19.3 , 220.4 ± 19.4 , 223.7 ± 19.6 , 239.4 ± 47.0 and 159.6 ± 9.3 $\text{mM}^{-1}\text{s}^{-1}$ for SMG-10, SMG-30, SHP-10, SHP-30, and Feridex, respectively. The r_2 values of all four formulas were significantly higher than Feridex (Table 2, $P < 0.05$). There was no statistical difference in r_2 values between 3.0 T and 7.0 T scanners for each IONP formula tested ($P > 0.05$).

***In vivo* Imaging**

Normal Balb/c mice were randomly divided into 5 groups and were each injected with one of the five formulas at a dose of 2.5 mg Fe/kg. T₂-weighted MRI was performed before and 10 min, 1 h, 24 h, 72 h, 1 wk and 2 wks post-injection in the 7.0 T small animal imaging system. Signal-to-noise ratios (SNRs) of the liver were derived (Fig. 4a) from MR images. All the formulas were found to quickly induce hypointensities in the liver. Except for SMG-10, all three other polymer coated formulas showed better contrast than Feridex at 10 min post injection at 7.0T at a dose of 2.5 mg Fe/kg ($P < 0.05$) (Fig. 4c and d, Table 3). Following our observation that particles with a 30 nm core size induced higher hypointensities than those with 10 nm cores at a dose of 2.5 mg Fe/kg, we further compared the contrast ability of SMG-30, SHP-30 and Feridex at a lower dose (1.0 mg Fe/kg). We found that all three formulas had a very similar trend of liver signal change, with SNR quickly reaching maximum within 10 min, and a long period of plateau up to 72 h p.i., followed by gradual restoration to the normal level in 2 weeks. Again, both SMG-30 and SHP-30 were more efficient in inducing hypointensities than Feridex at such a low dose ($P < 0.05$ at multi-time points) (Fig. 4b and e, Table 3). SHP-30 also tends to be cleared faster than SMG-30 from the liver, a property that is essential in reducing the potential toxicity of Fe. However, there is no statistical difference between the novel particles and Feridex at 2 weeks time point at the dose of 1.0 mg Fe/kg at 7.0T (Fig. 4e). To study the clinical potential of these IONPs, the contrast ability of the 5 formulas at clinical 3.0 T MR at a dose of 1.0 and 0.56 mg Fe/kg were tested and the results were similar to those obtained from 7.0 T small animal imaging system.

We then compared SHP-30 and Feridex in a Huh7 orthotropic model. We injected both formulas at a dose of 2.5 mg Fe/kg and acquired T₂-weighted images pre- as well as 10 min and 60 min post-injection from the 7.0 T small animal MRI system (Fig. 5). From the images, the CNRs were found to be 132.9 ± 21.2 and 146.6 ± 18.9 at 10 and 60 min p.i. for Feridex. This index improved to 149.3 ± 20.0 and 153.6 ± 23.0 at 10 and 60 min p.i. for SHP-30. Postmortem *ex vivo* Prussian blue staining found that most SHP-30 particles were trapped in the liver instead of tumor cells (Fig. 6).

DISCUSSION

Liver MRI is a key element in the diagnosis, management and follow-up of patients with hepatocellular disease, such as hepatocellular carcinoma (HCC). IONPs play a significant role in this context, as they are preferably taken up by Kupffer cells and induce hypointensities in the liver parenchyma. As a consequence, the visibility of lesions, such as metastases or HCC, is improved. Ideally, IONPs for such applications should have the following characteristics: 1) high magnetization value, which means better contrast and, therefore, a minimized dose; 2) size smaller than 100 nm, with a narrow size distribution for bolus intravenous administration, instead of slow intravenous infusion; and 3) appropriate coating to allow the magnetic particles to be stably suspended under physiological conditions and, simultaneously, to be non-toxic, non-immunogenic and be easily cleared from the body.

In the present study, we used pyrolysis to prepare IONPs with two core sizes (10 nm and 30 nm). TEM studies confirmed the size homogeneity of the particles. This high temperature treatment led to products with better crystallinity, and therefore higher magnetism, which explains their superiority over Feridex in r_2 relaxivity. Among the four polymer-coated formulas, we found that 30 nm nanoparticles possessed higher r_2 than the 10 nm ones. This is not surprising since magnetism is a function of nanoparticle size. On the other hand, we noticed that the difference is not dramatic. It could be attributed to the fact that the 10 nm IONPs already have a magnetism that is close to bulk materials. Hence, a further increase of

the particle size does not necessarily improve their contrast ability. Meanwhile, we found that the coating also had some effect on the r_2 values. Specifically, PEGylated formulas displayed smaller r_2 values than their corresponding non-PEGylated analogues of the same core size. A similar observation was made previously and was attributed to increased exclusion radius of protons (19).

As previously mentioned, the primary drawbacks of Feridex are their large hydrodynamic size and wide size distribution (20–22). These exclude their use as bolus injectable agents in the clinic. Instead, Feridex is primarily administered via infusion, which is suboptimal for routine clinical use. The polymer coated IONPs, on the other hand, are much smaller in overall size, despite of their larger core sizes. This is in part due to the better size control of the pyrolysis method, which leads to products with narrow size distributions. Moreover, the polymer coating efficiently encapsulates the particle cores and thus reduces the surface energy, and prevents the nanoparticles from aggregating.

One important feature required by the IONPs, when used as liver imaging contrast agents, is greater uptake by macrophages (Kupffer cells) than by tumor cells. Indeed, we found from the *in vitro* studies that all the formulas, including Feridex, showed similar levels of uptake by tumor cells (Huh 7), all of which were lower than those by macrophages (RAW 264.7). The coating strategy plays a significant role in determining the uptake level. Generally, the cellular uptake was found to follow the following order: SHP > Feridex > SMG. This is explained by the effect of surface charge, as measured by zeta potential analysis. The SHP nanoparticles are more negatively charged than Feridex (Table 1), and are therefore more likely to induce a scavenging response. The SMG nanoparticles, on the other hand, are protected with a layer of antifouling material, which greatly reduces their uptake level (23). When the coating is the same, the core particle size was found to affect the macrophage uptake to a certain degree. For both SHP and SMG, 30 nm cores were found to induce higher uptake than 10 nm cores. Overall, the *in vitro* studies showed that SHP-30 IONPs had both the highest r_2 value and the most prominent macrophage uptake.

The *in vivo* results are quite in accordance with the *in vitro* observations. From the tests in normal mice, we found that SMG-30 nanoparticles were merely comparable to Feridex in inducing hypointensities in liver at high doses (2.5 mg Fe/kg), and that SMG-10 was even less able than Feridex to induce such hypointensities. On the other hand, the SHP nanoparticles, especially SHP-30, were shown to be much more efficient in reducing the T_2 relaxation time. Notably, while SMG-30 had only a marginal advantage at 2.5 mg Fe/kg over Feridex, this lead in performance was greatly extended at clinical dose (0.56 mg Fe/kg). This confirmed our expectation that an advantage in contrast could lead to a reduced injection dose. The SMG-30 and SHP-30 showed comparable performance in terms of inducing liver hypointensities. However, the latter showed a faster clearance rate, which is a highly preferred attribute for allowing longitudinal studies on the same living subject and potentially for lower liver toxicity. In addition, *in vivo* studies on an orthotropic Huh7 HCC tumor model further confirmed the superiority of SHP-30 over Feridex in improving lesion visibility.

The emerging field of nanotechnology has provided a means to improve traditionally used, IONP-based MRI contrast probes. There have been few systematic studies to investigate how particle core size, hydrodynamic size, surface charge and PEGylation can affect a particle's role as a contrast agent in liver cancer imaging. Indeed, by tuning the parameters of IONPs, we can arrive at formulas that are injectable i.v., offer fast clearance from the body, and can induce high contrast between normal liver and HCC lesions.

CONCLUSION

We report in this manuscript the evaluation of superparamagnetic IONPs of different coatings (SMG and SHP) and core sizes (10 nm and 30 nm) for liver MR imaging. Synthesized by pyrolysis, these IONP formulas possess higher r_2 relaxivity than Feridex. Through *in vitro* studies, we were able to identify one formula, SHP-30, with the best contrast and highest macrophage uptake. *In vivo*, SHP-30 outperformed Feridex as a contrast probe in both normal mice and in an Huh7 orthotopic tumor model. The success of this study suggests that the SHP-30 formula might be an improved alternative to Feridex for liver imaging as an i.v. contrast agent.

Acknowledgments

This work was supported in part, by the intramural research program of the National Institute of Biomedical Imaging and Bioengineering (NIBIB), NIH and NIH SBIR/STTR program (HHSN261200800062C and 1R41CA137960), the International Cooperative Program of the National Science Foundation of China (NSFC) (81028009), and by the International Cooperation Projects of the Chinese Ministry of Sciences and Technology (2009DFB30040). Dr. Jin Xie was partially supported by the NIH Pathway to Independence (K99/R00) Award. The authors wish to thank Mrs. Yan Hou from Harbin Medical University for statistical analysis.

References

1. Xie J, Huang J, Li X, Sun S, Chen X. Iron oxide nanoparticle platform for biomedical applications. *Curr Med Chem*. 2009; 16:1278–1294. [PubMed: 19355885]
2. Poeckler-Schoeniger C, Koepke J, Gueckel F, Sturm J, Georgi M. MRI with superparamagnetic iron oxide: efficacy in the detection and characterization of focal hepatic lesions. *Magn Reson Imaging*. 1999; 17:383–392. [PubMed: 10195581]
3. Ward J, Guthrie JA, Wilson D, Arnold P, Lodge JP, Toogood GJ, Wyatt JI, Robinson PJ. Colorectal hepatic metastases: detection with SPIO-enhanced breath-hold MR imaging--comparison of optimized sequences. *Radiology*. 2003; 228:709–718. [PubMed: 12888620]
4. Xie J, Lee S, Chen X. Nanoparticle-based theranostic agents. *Adv Drug Deliv Rev*. 2010; 62:1064–1079. [PubMed: 20691229]
5. Bhirde A, Guo N, Chen X. Targeted nanoprobe reveal early time point kinetics *in vivo* by time-resolved MRI. *Theranostics*. 2011; 1:274–276. [PubMed: 21562633]
6. Kessinger CW, Togao O, Khemtong C, Huang G, Takahashi M, Gao J. Investigation of *in vivo* targeting kinetics of alpha(v)beta(3)-specific superparamagnetic nanoprobe by time-resolved MRI. *Theranostics*. 2011; 1:263–273. [PubMed: 21562632]
7. Tan M, Lu ZR. Integrin targeted MR imaging. *Theranostics*. 2011; 1:83–101. [PubMed: 21547154]
8. Yallapu MM, Foy SP, Jain TK, Labhasetwar V. PEG-functionalized magnetic nanoparticles for drug delivery and magnetic resonance imaging applications. *Pharm Res*. 2010; 27:2283–2295. [PubMed: 20845067]
9. Maeng JH, Lee DH, Jung KH, Bae YH, Park IS, Jeong S, Jeon YS, Shim CK, Kim W, Kim J, Lee J, Lee YM, Kim JH, Kim WH, Hong SS. Multifunctional doxorubicin loaded superparamagnetic iron oxide nanoparticles for chemotherapy and magnetic resonance imaging in liver cancer. *Biomaterials*. 2010; 31:4995–5006. [PubMed: 20347138]
10. Das M, Dhak P, Gupta S, Mishra D, Maiti TK, Basak A, Pramanik P. Highly biocompatible and water-dispersible, amine functionalized magnetite nanoparticles, prepared by a low temperature, air-assisted polyol process: a new platform for bio-separation and diagnostics. *Nanotechnology*. 2010; 21:125103. [PubMed: 20195015]
11. Xie J, Liu G, Eden HS, Ai H, Chen X. Surface-engineered magnetic nanoparticle platforms for cancer imaging and therapy. *Acc Chem Res*. 2011; 44:883–892. [PubMed: 21548618]
12. Essig M. Protocol design for high relaxivity contrast agents in MR imaging of the CNS. *Eur Radiol*. 2006; 16(Suppl 7):M3–M7. [PubMed: 18655261]

13. Kunzmann A, Andersson B, Thurnherr T, Krug H, Scheynius A, Fadeel B. Toxicology of engineered nanomaterials: Focus on biocompatibility, biodistribution and biodegradation. *Biochim Biophys Acta*. 2011; 1810:361–373. [PubMed: 20435096]
14. Laurent S, Forge D, Port M, Roch A, Robic C, Vander Elst L, Muller RN. Magnetic iron oxide nanoparticles: synthesis, stabilization, vectorization, physicochemical characterizations, and biological applications. *Chem Rev*. 2008; 108:2064–2110. [PubMed: 18543879]
15. Ho D, Sun X, Sun S. Monodisperse magnetic nanoparticles for theranostic applications. *Acc Chem Res*. 2011; 44:875–882. [PubMed: 21661754]
16. Park J, Lee E, Hwang NM, Kang MS, Kim SC, Hwang Y, Park JG, Noh HJ, Kini JY, Park JH, Hyeon T. One-nanometer-scale size-controlled synthesis of monodisperse magnetic iron oxide nanoparticles. *Angew Chem Int Ed*. 2005; 44:2872–2877.
17. Yu WW, Falkner JC, Yavuz CT, Colvin VL. Synthesis of monodisperse iron oxide nanocrystals by thermal decomposition of iron carboxylate salts. *Chem Commun (Camb)*. 2004:2306–2307. [PubMed: 15489993]
18. Duan H, Kuang M, Wang X, Wang A, Mao H, Nie S. Reexamining the effects of particle size and surface chemistry on the magnetic properties of iron oxide nanocrystals: new insights into spin disorder and proton relaxivity. *J Phys Chem C*. 2008; 112:8127–8131.
19. LaConte LE, Nitin N, Zurkiya O, Caruntu D, O'Connor CJ, Hu X, Bao G. Coating thickness of magnetic iron oxide nanoparticles affects R2 relaxivity. *J Magn Reson Imaging*. 2007; 26:1634–1641. [PubMed: 17968941]
20. Kaim AH, Wischer T, O'Reilly T, Jundt G, Frohlich J, von Schulthess GK, Allegrini PR. MR imaging with ultrasmall superparamagnetic iron oxide particles in experimental soft-tissue infections in rats. *Radiology*. 2002; 225:808–814. [PubMed: 12461265]
21. Lee HY, Lee SH, Xu C, Xie J, Lee JH, Wu B, Koh AL, Wang X, Sinclair R, Wang SX, Nishimura DG, Biswal S, Sun S, Cho SH, Chen X. Synthesis and characterization of PVP-coated large core iron oxide nanoparticles as an MRI contrast agent. *Nanotechnology*. 2008; 19:165101. [PubMed: 21394237]
22. Huang J, Bu L, Xie J, Chen K, Cheng Z, Li X, Chen X. Effects of nanoparticle size on cellular uptake and liver MRI with polyvinylpyrrolidone-coated iron oxide nanoparticles. *ACS Nano*. 2010; 4:7151–7160. [PubMed: 21043459]
23. Zhu L, Xie J, Swierczewska M, Zhang F, Quan Q, Ma Y, Fang X, Kim K, Lee S, Chen X. Real-time video imaging of protease expression in vivo. *Theranostics*. 2011; 1:18–27. [PubMed: 21461134]

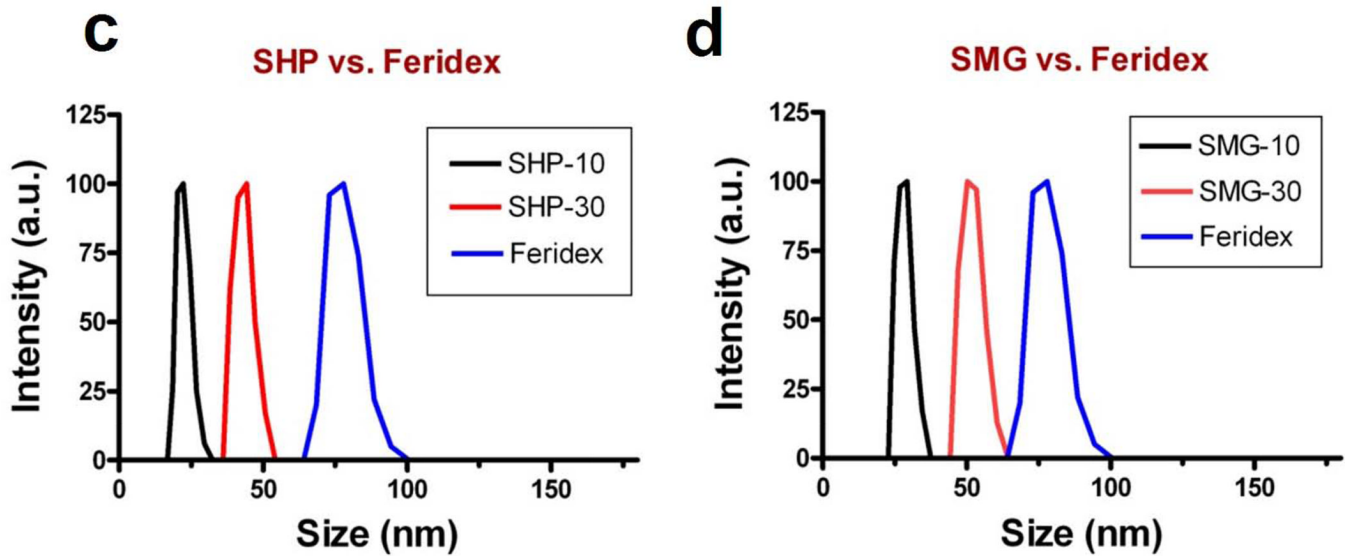
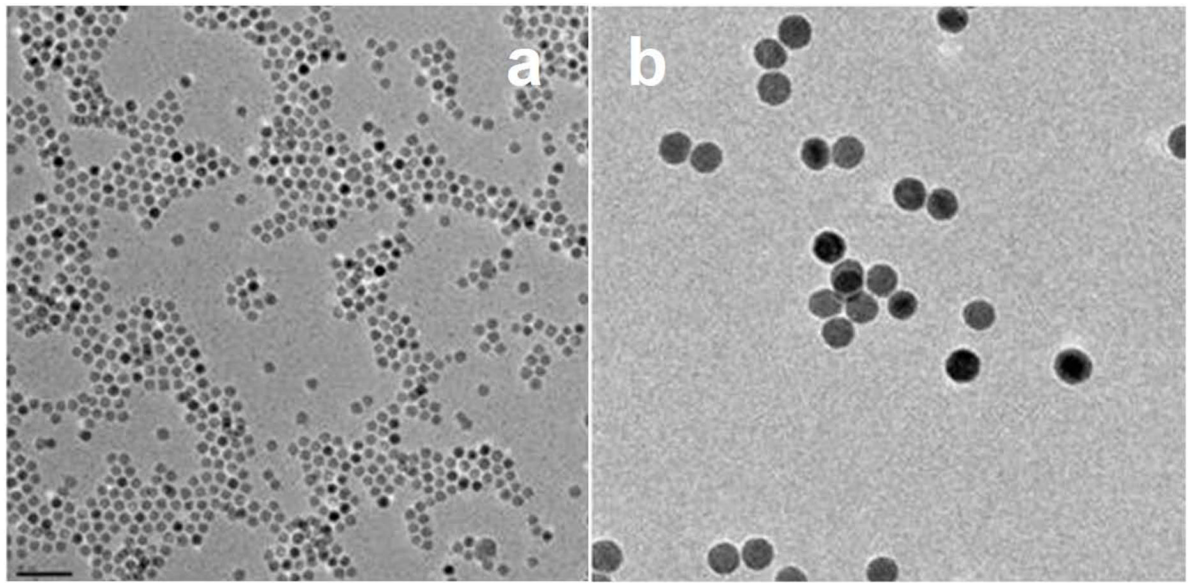


Figure 1. TEM images of representative (a) 10 nm and (b) 30 nm IONPs prepared via pyrolysis, and dynamic light scattering results of (c) SHP and (d) SMG IONPs.

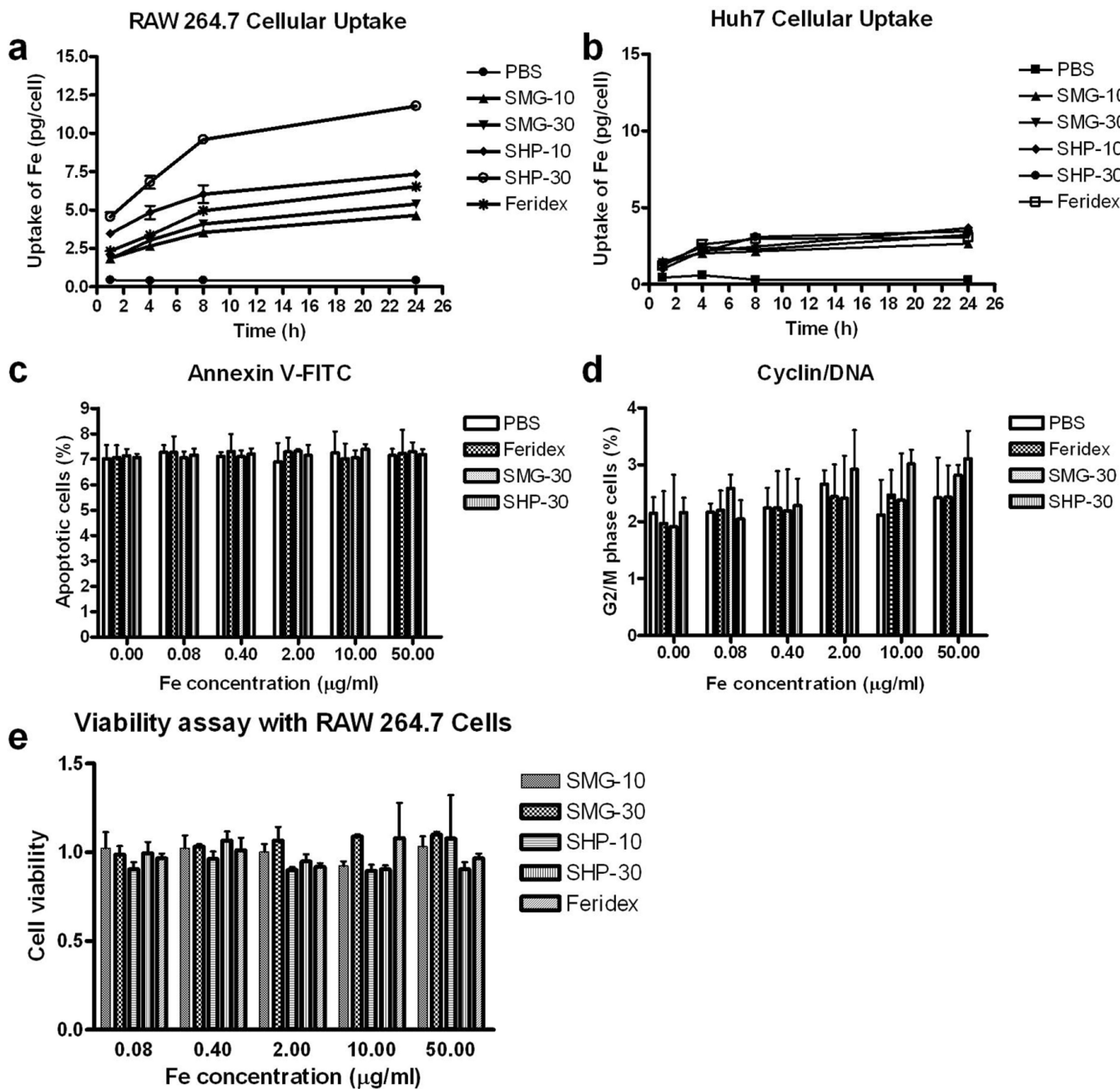


Figure 2. Cellular uptake of different types of IONPs by (a) RAW 264.7 macrophage cells and (b) Huh7 human hepatocellular carcinoma cells. (c and d) apoptosis (c) and cyclin/DNA (d) flow cytometry assays with RAW 264.7 macrophage cells. (e) Cell viability assay with RAW 264.7 macrophage cells.

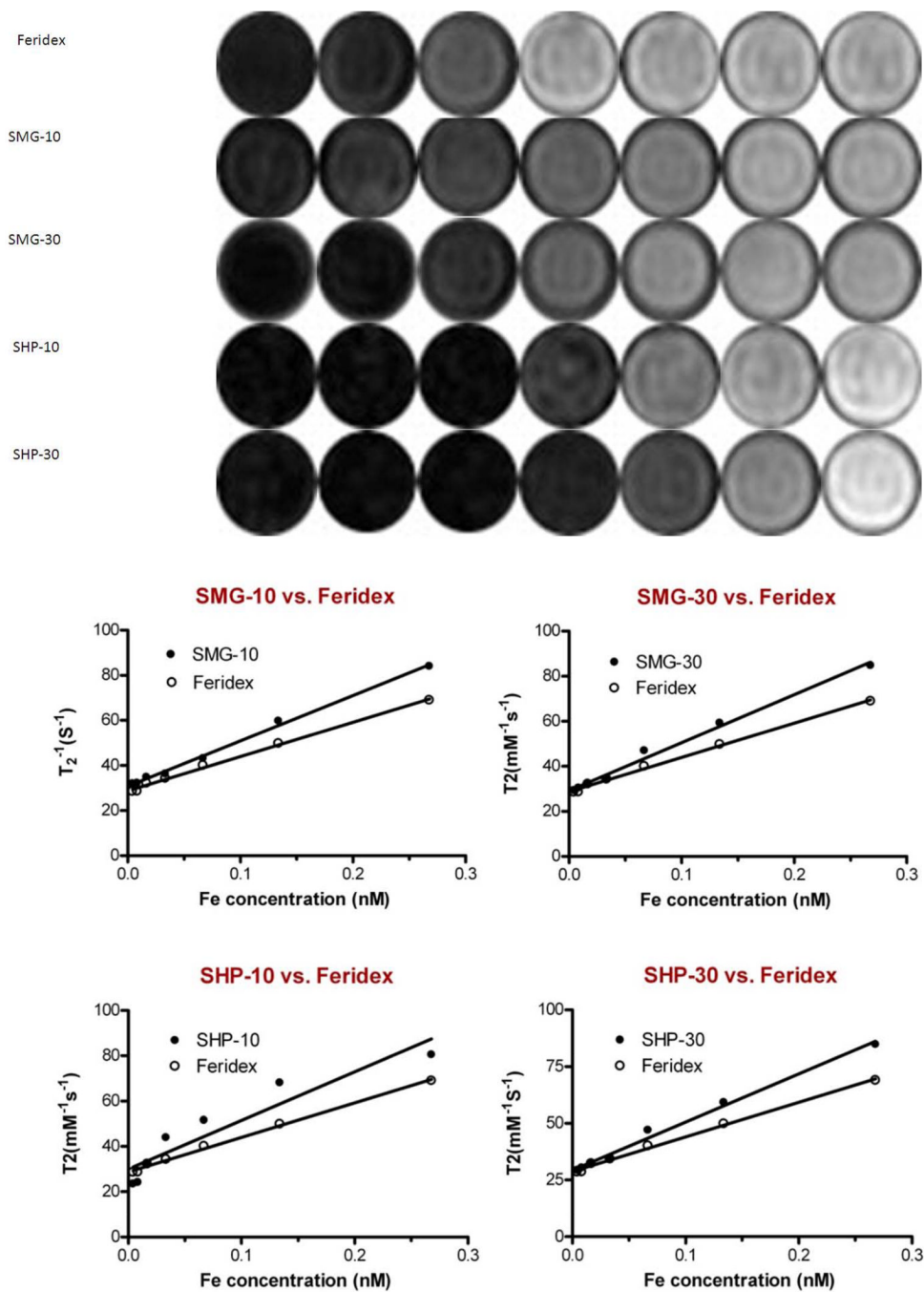


Figure 3.

(a) T₂-weighted phantom images of the IONPs as a function of iron concentrations. (b–e) r₂ relaxivities derived from 1/T₂ vs. [Fe] curves. The r₂ values were calculated to be 201.5 ± 7.1, 212.7 ± 5.8, 214.2 ± 3.8, 230.3 ± 1.5 and 152.2 ± 2.5 mM⁻¹s⁻¹ for SMG-10, SMG-30, SHP-10, SHP-30 and Feridex, respectively (n = 3).

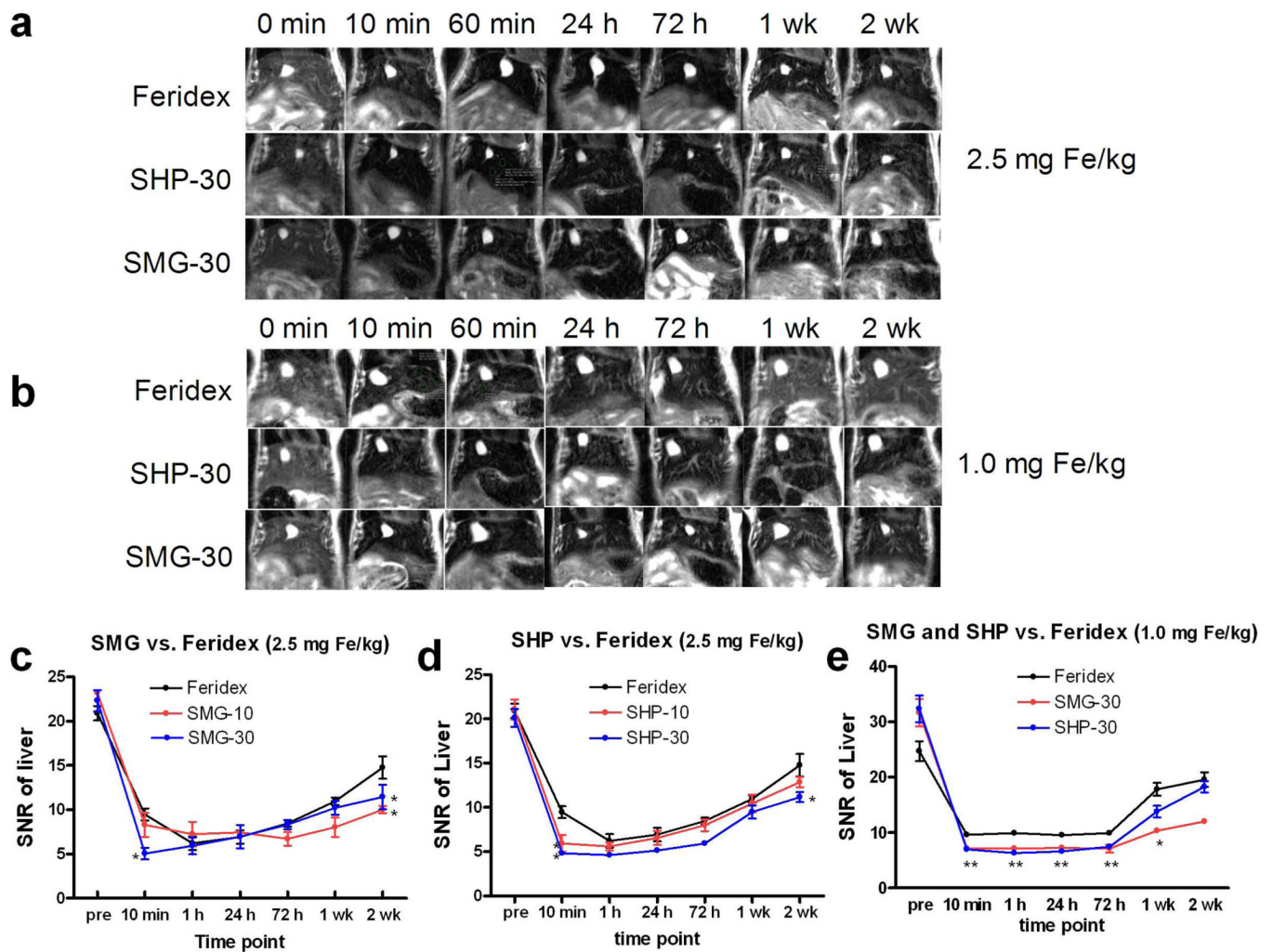


Figure 4.

(a–b) Representative T₂-weighted MR images of normal Balb/c mice before and 10 min, 24 h, 72 h, 1 wk and 2 wks after tail-vein injection of SHP-30, SMG-30 and Feridex at a dose of 2.5 mg Fe/kg (a) and 1.0 mg Fe/kg (b) using a 7.0 T small animal MRI system. (c–d) SNR vs. time curves of different nanoparticles at the dose of 2.5 mg Fe/kg. Among all the formulas, SHP-30 showed the best efficacy in inducing hypointensities in liver parenchyma. (e) SNR vs. time curves of SHP-30, SMG-30 and Feridex at the dose of 1.0 mg Fe/kg using a 7.0 T small animal MRI system. *, P < 0.05; **, P < 0.01.

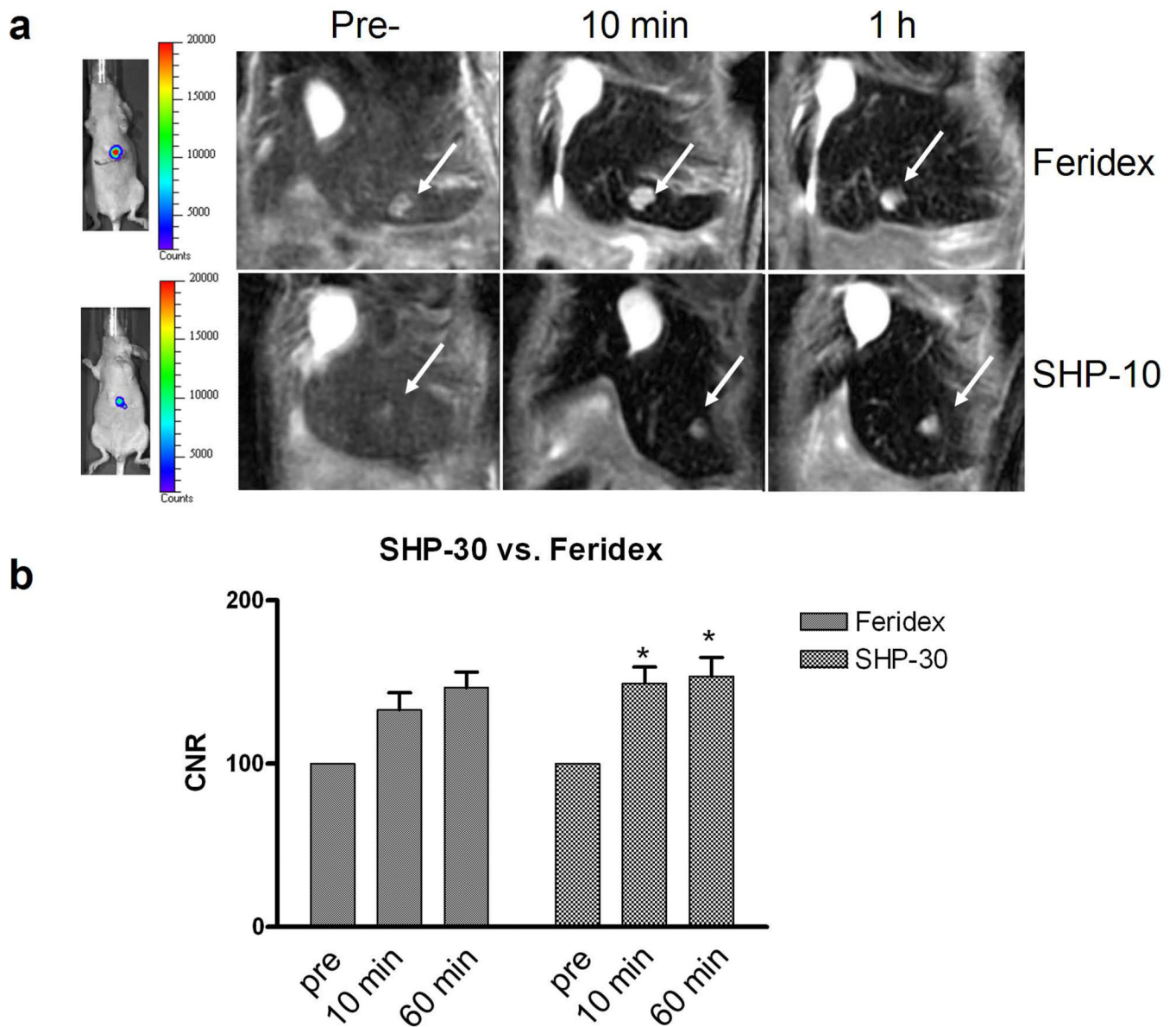


Figure 5.

(a) BLI (left) and MRI (right) of representative Huh7 tumor-bearing mice injected with Feridex or SHP-30 at a dose of 2.5 mg Fe/kg using a 7.0 T small animal MRI system. The images were taken coronally before and 10 min, 1 h after particle injection. (b) The CNR of Feridex and SHP-30 at before and 10 min, 1 h after particle injection. SHP-30 showed higher CNR than Feridex at both time points after particle injection. *, $P < 0.05$.

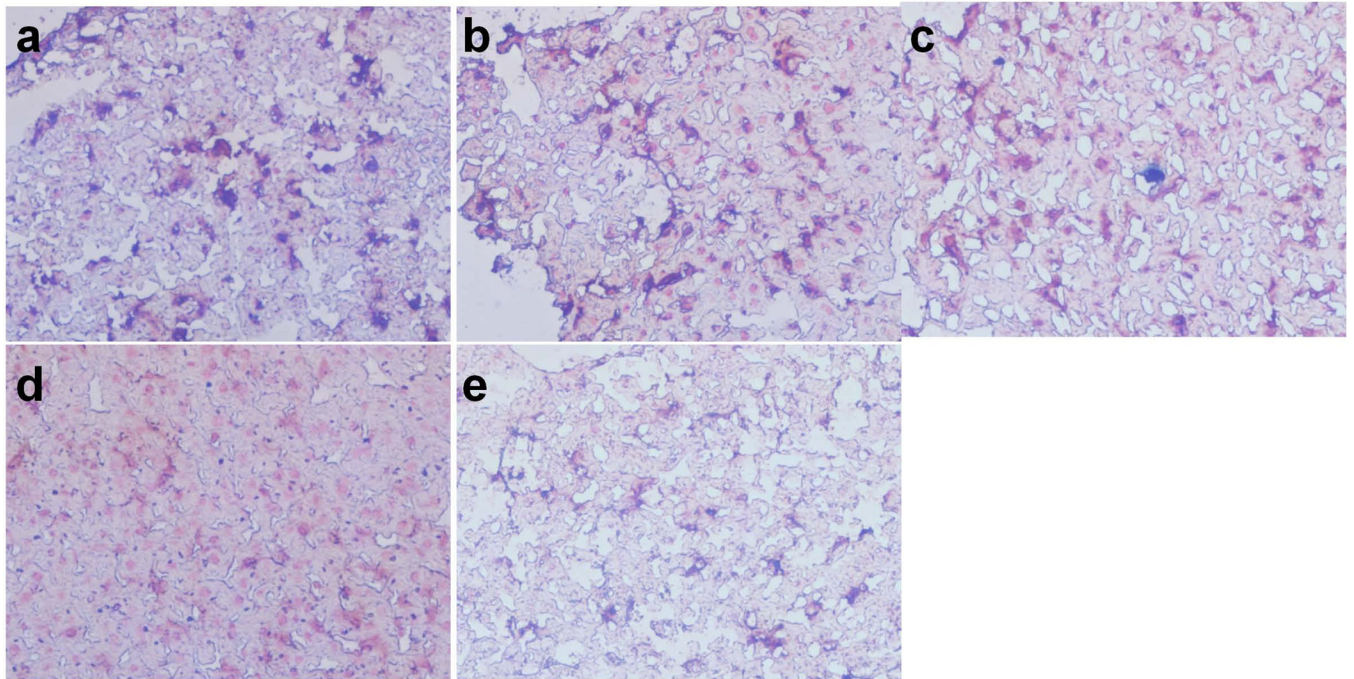


Figure 6. F4/80 and Prussian blue double staining of liver tissue slices at 24 h after tail vein injection of IONPs as well as Feridex (40 \times). (a) Feridex, (b) SHP-30, (c) SMG-30, (d) SHP-10 and (e) SMG-10.

Table 1

Characterizations of Polymer Coated IONPs.

	Core size (nm)	Overall Size (nm)	Zeta potential (mV)
SHP-10	10	23.1	-45.01
SHP-30	30	25.0	-47.52
SMG-10	10	49.1	-14.99
SMG-30	30	63.8	-6.22
Feridex	5	85-120	-21.60

Table 2

R₂ value of IONPs at different magnetic field strengths with the same concentration.

IONPs	magnetic strength	
	7.0 T	3.0 T
SMG-30	212.68 ± 5.75 *	220.07 ± 9.54 *
SMG-10	201.54 ± 7.09 *	210.49 ± 5.50 *
SHP-30	230.22 ± 1.47 *	239.41 ± 6.60 *
SHP-10	214.16 ± 3.84 *	222.81 ± 15.81 *
Feridex	152.21 ± 2.52	159.88 ± 8.12

* (AVG±SD of 3 measurements, P < 0.05 as compared to Feridex).

Table 3

The liver contrast-to-noise ratio (CNR) at different IONP doses under different magnetic field strengths.

	Magnetic strength	Dose (mg/kg)	Time							
			0 min	10 min	60 min	24 h	72 h	1 wk	2 wk	
SMG-10	7.0T	2.5	23.19±0.55	8.30±2.34	7.24±2.41	7.45±0.45	6.72±1.34	8.03±1.87	10.02±0.73 ^Δ	
	3.0T	0.56	15.78±1.70	12.27±2.54	9.69±1.09	8.04±1.07 [*]	10.08±3.35	11.28±1.71 [*]	12.50±3.32	
	7.0T	2.5	22.31±2.09	5.05±1.13 ^Δ	5.93±1.66	6.97±2.27	8.32±0.86	10.22±1.33	11.44±2.39 ^Δ	
SMG-30	7.0T	1.0	31.66±4.31	7.15±0.78 [§]	7.13±0.38 [§]	7.25±0.52 [§]	7.11±1.27 [§]	10.36±0.93 [§]	12.02±0.73	
	3.0T	1.0	18.71±2.74 [#]	8.46±3.65	8.38±1.47	6.00±1.45	8.02±1.18	12.46±0.83	13.08±4.55	
	7.0T	0.56	19.64±0.40	9.33±0.89	7.36±1.93 [*]	6.72±2.39 [*]	10.37±1.51 [*]	12.59±0.87	14.01±3.73	
SHP-10	7.0T	2.5	21.06±1.94	5.93±1.66 ^Δ	5.59±0.79	6.55±1.39	7.98±1.16	10.45±1.73	12.85±0.99	
	3.0T	0.56	19.69±5.87	11.84±2.82	8.48±1.13 [*]	7.98±0.75 [*]	8.84±1.66 [*]	14.56±1.58	15.62±1.34	
	7.0T	2.5	20.10±1.73	4.83±0.39 ^Δ	4.61±0.09 ^Δ	5.14±0.22 ^Δ	5.93±0.54 ^Δ	9.48±1.29	11.15±0.97 ^Δ	
SHP-30	7.0T	1.0	32.34±4.17	6.98±0.60	6.32±0.20	6.61±0.58	7.46±0.78 [§]	13.81±1.81	18.26±1.74	
	3.0T	1.0	20.83±1.83 [#]	12.22±1.54	10.75±1.01	7.48±1.65	11.81±1.95	14.23±2.64	18.85±2.91	
	7.0T	0.56	19.78±0.89	12.67±0.26	8.52±0.28 [*]	7.66±1.44 [*]	9.9±2.08 [*]	14.14±2.5	15.67±1.22	
Feridex	7.0T	2.5	20.90±1.42	9.48±1.16	6.22±1.32 ^Δ	6.94±1.30	8.48±0.65	10.97±0.72	14.77±2.20	
	1.0	26.18±2.23	9.63±0.82	9.91±0.42	9.54±0.26	9.92±0.40	17.80±2.02	19.57±2.26 [#]		
	3.0T	1.0	19.50±1.63 [#]	13.92±1.86	13.96±1.03	14.04±4.01	15.51±3.11	17.76±8.92	19.75±7.48	
		0.56	16.09±2.29	10.67±2.90	10.59±0.54	13.51±2.84	14.97±2.06	15.04±1.5	16.83±3.98	

* P < 0.05 for Feridex vs. IONPs at 3.0 T and 0.56 mg Fe/kg;

P < 0.05 for 3.0 T vs. 7.0 T at 1.0 mg Fe/kg;

Δ P < 0.05 for Feridex vs. IONPs at 7.0 T and 2.5 mg Fe/kg;

§ P < 0.05 for Feridex vs. SHP-30/SMG-30 at 7.0 T and 1.5 mg Fe/kg.